Seismic collapse risk of RC frames with irregular distributed masonry infills

Yan-Wen Li[1], Michael C.H. Yam[1] and Ke Cao[*2]

[1] Department of Building and Real Estate, The Hong Kong Polytechnic University, Hung Hom, Kowloon, Hong Kong SAR, China
[2] School of Management Science and Real Estate, Chongqing University, Chongqing 400044, China

(Received keep as blank , Revised keep as blank , Accepted keep as blank)

Abstract. Masonry infills are normally considered as non-structural elements in design practice, therefore, the interaction between the bounding frame and the strength contribution of masonry infills is commonly ignored in the seismic analysis work of the RC frames. However, a number of typical RC frames with irregular distributed masonry infills have suffered from undesirable weak-story failure in major earthquakes, which indicates that ignoring the influence of masonry infills may cause great seismic collapse risk of RC frames. This paper presented the investigation on the risk of seismic collapse of RC frames with irregularly distributed masonry infills through a large number of nonlinear time history analyses (NTHAs). Based on the results of NTHAs, seismic fragility curves were developed for RC frames with various distribution patterns of masonry infills. It was found that the existence of masonry infills generally reduces the collapse risk of the RC frames under both frequent happened and very strong earthquakes, however, the severe irregular distribution of masonry infills, such as open ground story scenario, results in great risk of forming a weak story failure. The strong-column weak-beam (SCWB) ratio has been widely adopted in major seismic design codes to control the potential of weak story failures, where a SCWB ratio value about 1.2 is generally accepted as the lower limit. In this study, the effect of SCWB ratio on inter-story drift distribution was also parametrically investigated. It showed that improving the SCWB ratio of the RC frames with irregularly distributed masonry infills can reduce inter-story drift concentration index under earthquakes, therefore, prevent weak story failures. To achieve the same drift concentration index limit of the bare RC frame with SCWB ratio of about 1.2, which is specified in ACI318-14, the SCWB ratio of masonry-infilled RC frames should be no less than 1.5. For the open ground story scenario, this value can be as high as 1.8.

Keywords: seismic collapse; weak story failure; seismic fragility curves; Nonlinear time history analysis; strong-column weak-beam ratio.

1. Introduction

Masonry infills have been widely used in multi-story reinforced concrete (RC) frames owing to their cost-effectiveness and excellent heat and acoustical insulation characteristics. For many multi-story buildings in prime business areas, the upper stories are designed for residential purposes, while the ground stories are designed for commercial purposes, such as shopping centers, restaurants and gymnasiums. The commercial areas usually need large space and results in open bays or open stories in the ground floor, while the residential areas in the upper stories usually employ masonry infills to separate individual private spaces, therefore the irregular distribution of masonry infills are widely existed in practice.

The masonry infills are normally considered as non-structural elements in design practice (ASCE7-10, 2013; Eurocode8, 2005; GB 50011-2010, 2010; IBC2000, 2000), thus the interaction between the bounding frame and the strength contribution of masonry infills to the structural system is commonly ignored in seismic analysis of the structural system. Seismic design of RC frames is usually based on the bare frame system composed of beam and column elements. Accordingly, the strong column-weak beam criterion proposed by Paulay and Priestley (Paulay and Priestley, 1992) is applied to achieve the ductile global failure pattern rather than the soft/weak story failure pattern under earthquakes. However, a large number of conventional code-compliant RC frames with masonry infills have suffered from undesirable weak-story failure in major earthquakes, such as the Mexico City earthquake in 1985 and the Wenchuan earthquake in 2008 (Verde, 1991; Zhao et al., 2009). Previous experimental and analytical works have shown that the existence of masonry infills enhances the stiffness and strength of RC frames, which results in an amplifed seismic action (P G Asteris et al., 2017; Panagiotis G. Asteris et al., 2015; Khoshnoud & Marsono, 2016; Muthukumar et al., 2017; Papia et al., 2003; Sandhu et al., 2020). In particular, irregular distribution of masonry infills changes the story stiffness and strength along the structural height. Consequently, the story drifts will concentrate in a soft/weak story under earthquakes, which results in weak story collapse (Li et al., 2018).

Considerable research has been conducted in an effort to investigate the performance of frame structures and the bounding frame - masonry infills interaction under earthquakes. Huang et al. (Huang et al., 2016) experimentally investigated the seismic performance of RC frames with and without masonry infills. It was found that both the elastic stiffness and ultimate capacity of the masonry-infilled RC frames were significantly higher than those of bare frames, as shown in Fig. 1. Yuen and Kuang (Yuen and Kuang, 2015) investigated the seismic response and failure mechanism of masonry-infilled RC frames using three-dimensional discrete element method. The results indicated that full height and continuous-infill panels can enhance the seismic performance of framed structures, while discontinuous infills can cause serious damage concentration at the points of discontinuity due to the short column effect (Bikce, 2011). Moreover, the results revealed that the design concept of "strong column-weak beam" may not be always applicable to masonry-infilled RC frames.

Evaluating the seismic performance of new buildings require an accurate assessment of seismic collapse risk of buildings considering the contribution of masonry infills (Haselton et al., 2011). Advances in nonlinear time history analysis and performance-based earthquake engineering have provide great impetus for development of seismic collapse risk assessment of structural systems (Burton and Deierlein, 2014). In recent years, the development of macro numerical models for masonry infills (De Domenico et al., 2018; Mohammad Noh et al., 2017) has enabled comprehensive studies on the nonlinear seismic responses of masonry-infilled RC frames. However, these previous studies focused on the seismic performance of single masonry-infilled RC frame with opening ground story, opening doors and opening windows (Quayyum et al., 2013b). The effect of various irregularly distributed masonry infills, such as open ground stories and open bays in some stories, on the global seismic response of RC frames has not been reported yet.

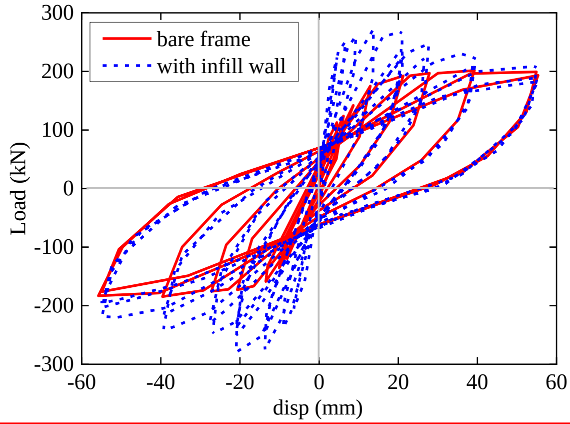

Fig. 1 Lateral load versus displacement of RC frame with and without masonry infills (Huang et al., 2016)

The main objective of this study is to investigate the seismic collapse risk of RC frames with irregular distributed masonry infills. To this end, a six-story code-compliant RC frame with masonry infills is adopted as the prototype frame in this study. Six distribution scenarios of masonry infills are considered, including (1) full infilled, (2) open first/ground story, (3) open second story, (4) continuous open one bay in ground two stories, (5) staged open one bay in ground two stories, and (6) bare frame. In general, these structural types cover most masonry infill distribution scenarios of RC frames. Two-dimensional nonlinear numerical models of the prototype frame are developed using OpenSees (Mazzoni et al., 2006). Typical failure modes of the masonry infill panels were considered in the macro equivalent numerical model. Seismic fragility curves were developed based on the results of nonlinear time history analyses (NTHAs). For each model of the RC frame, the uncertainties in material properties and ground motions were considered. Moreover, the effect of the key design parameter, strong-column weak-beam ratio defined as the column-to-beam flexural strength ratio, on seismic response and failure mechanism of masonry-infilled RC frames are also investigated through the parametric study.

2. Development of numerical models

2.1 Modelling of masonry-infilled RC frames

Refined nonlinear numerical modelling approaches for masonry-infilled RC frames, such as three-dimensional finite element method and discrete element method, are usually accurate but costly in effort and computational time. Typical simplified analytical models such as the diagonal equivalent strut model, the single diagonal strut model and the multiple strut model are widely used as an alternative for evaluating seismic performance of masonry-infilled RC frames. In this study, the equivalent diagonal strut macro model proposed by Nurbaiah et al. (Mohammad Noh et al., 2017) was adopted to simulate the seismic behavior of masonry infill panels, as shown in Fig. 2. Reliable force-displacement relationships are required to simulate the seismic behavior of the equivalent strut. As illustrated in Fig. 2(b), Liberatore and Decanini (Liberatore and Decanini, 2011) proposed a four-line backbone curve for the strut compression behavior without considering the tension capacity. Line O-F represents the un-cracked phase with H_{mf} representing the crack capacity. Line F-FC corresponds to the post-cracking capacity development with H_{mfc} representing the ultimate capacity. The secant stiffness K_{mfc} of the strut in the horizontal direction at the complete cracking stage can be determined as,

$$K_{mfc} = \frac{E_m t_m b_m}{d_m} \cos^2 \theta \tag{1}$$

where E_m is the elastic modulus of the infill, t_m, b_m, d_m and θ are the thickness, width, length and incidence angle of the equivalent strut, respectively. All the parameters can be determined using the geometric and mechanical characteristics of masonry infills (Mohammad Noh et al., 2017).

To determine the ultimate capacity of masonry infills, four possible failure modes and the corresponding stresses were considered (Burton and Deierlein, 2014; Mohammad Noh et al., 2017), including (a) diagonal tension, H_{dt}; (b) diagonal compression, H_{dc}; (c) sliding shear, H_{ss}; and (d) corner crushing, H_{cc}. The equivalent failure stresses of these failure modes can be expressed as,

$$H_{dt} = \frac{0.6\tau_{m0} + 0.3\sigma_0}{b_m / d} \tag{2}$$

$$H_{dc} = \frac{1.16\tan\theta}{K_1 + K_2\lambda_h}\sigma_{m0} \tag{3}$$

$$H_{ss} = \frac{(1.2\sin\theta + 0.45\cos\theta)\tau_0 + 0.3\sigma_0}{b_m / d} \tag{4}$$

$$H_{cc} = \frac{1.12\sin\theta\cos\theta}{K_1\lambda_h^{-0.12} + K_2\lambda_h^{0.88}}\sigma_{m0} \tag{5}$$

where σ_{m0} is the compressive strength obtained from the vertical compression tests; σ_0 is the compressive stress induced by the gravity loads; τ_{m0} is the shear strength obtained from the diagonal compression tests; τ_0 is the sliding resistance in the joints obtained from empirical equations (herein, τ_0=0.7τ_{m0}) or tests.

Then, the minimum value among the four failure modes is conservatively adopted to calculate the lateral strength of the equivalent strut,

$$H_{mfc} = b_m t_m \cos\theta \cdot \min(H_{dt}, H_{dc}, H_{ss}, H_{cc}) \tag{6}$$

Line FC-R in Fig. 2(b) defines the stiffness and strength deterioration phase. Referring to (Mohammad Noh et al., 2017), the degrading stiffness K_2 and residual strength H_{mr} are adopted as 0.02K_{mfc} and 0.35H_{mfc}, respectively.

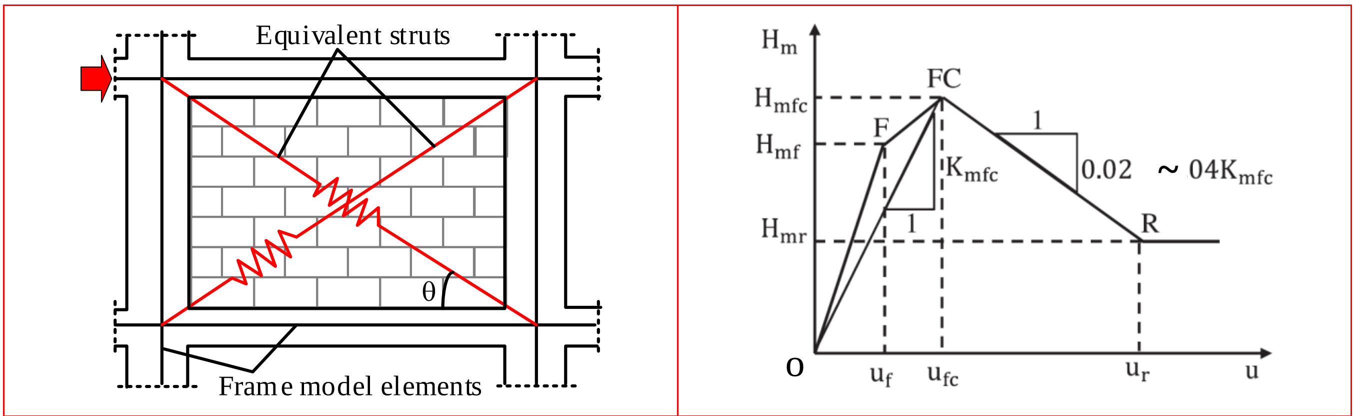

(a) model configuration (Mohammad Noh et al., 2017) | (b) backbone curve (Liberatore and Decanini, 2011)

Fig. 2 Macro model of the masonry infill panels

The uniaxialMaterial Concrete01 in OpenSees is a concrete material class with degraded linear unloading/reloading stiffness and without tensile strength, as shown in Fig.3. This material class is represented by four parameters including the ultimate stress, the strain at ultimate stress, the maximum strain and the stress at maximum strain. In this study, these input parameters of Concrete01 were calibrated with Eq. (1) and (6) to simulate the hysteretic behavior of the masonry infills.

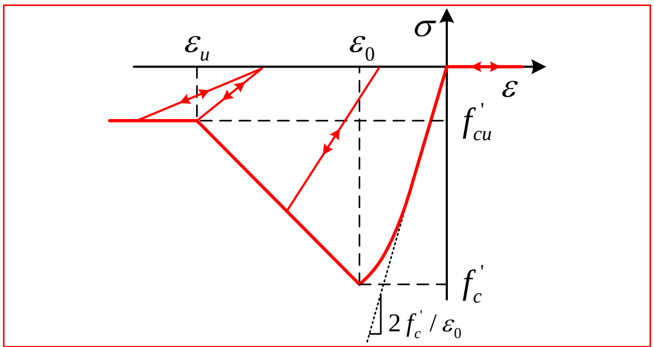

Fig. 3 Concrete01 uniaxial material model in OpenSees.

As shown in Fig. 4, the ForceBeamColumn elements with concentrated fiber plastic hinge at both ends in OpenSees (Mazzoni et al., 2006) were used to simulate the frame beams and columns. This class of force-based fiber elements can simulate the nonlinear behavior of a RC beam or column without mesh subdivision and allows the user to specify plastic hinge length at its ends. In this study, the length of plastic hinges at the ends of each element were set equal to the section height with reference to (Scott and Fenves, 2006). Two-point Gauss integration was used in the element interior while two-point Gauss-Radau integration was applied over the length of Lp_i and Lp_j at the element ends. The fiber section approach in the plastic hinge is also illustrated in Fig. 4. The concrete and reinforcing bars in the frame beams and columns were simulated with the uniaxialMaterial Concrete02 and Steel02, respectively, as shown in Fig. 4.

In the numerical model of RC frames, a load combination of 1.0DL+0.5LL was adopted as the gravity loads, wherein DL and LL are the standard values of floor dead and live loads, respectively. Gravity loads from the slabs are assigned as distributed loads on the main beams, while gravity loads from the transverse beams are assigned as concentrated loads on the beam-to-column joint nodes. All masses are lumped at the beam-to-column joint nodes and the flexible foundation effect is not considered in this study.

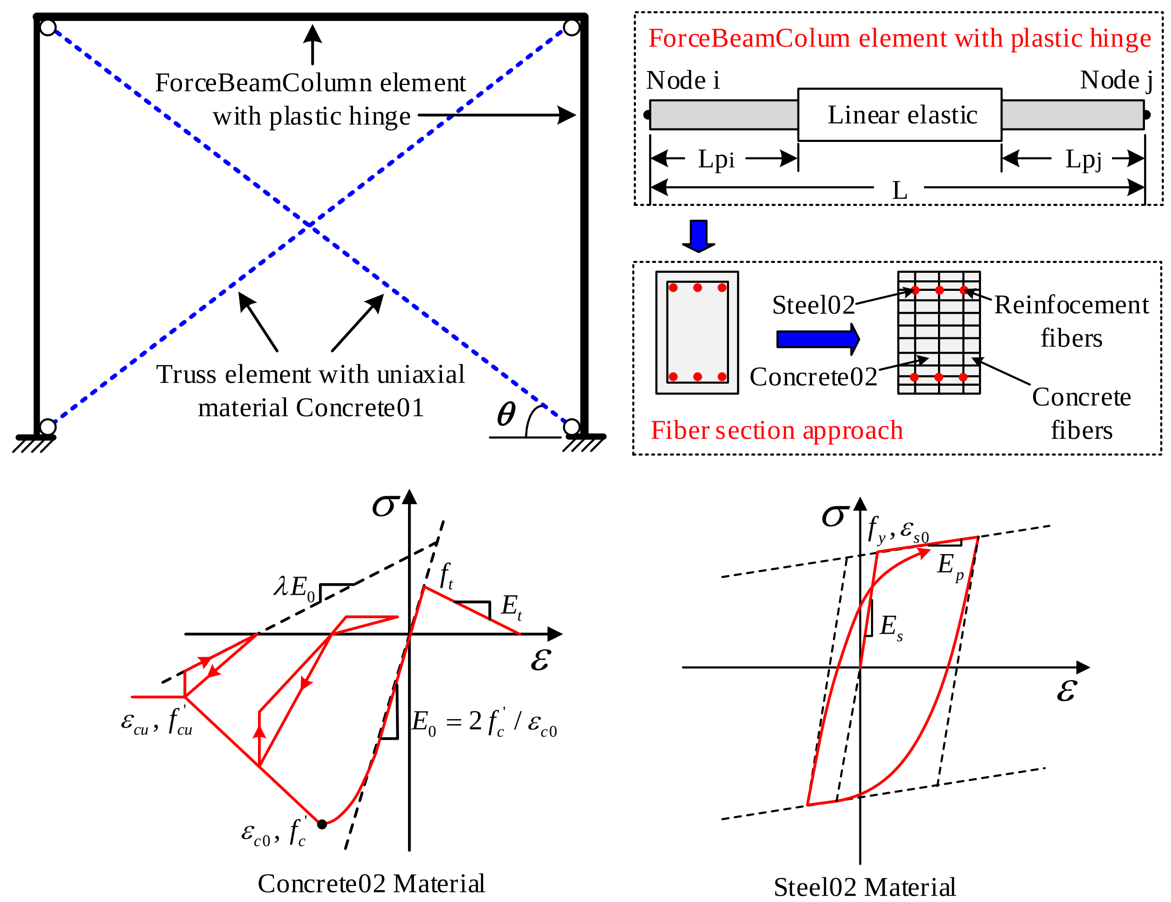

Fig. 4 Schematic of the equivalent strut model for masonry-infilled RC frames.

2.2 Model validation

The numerical model of masonry-infilled RC frames was validated against four experimental specimens, including one bare RC frame and three masonry-infilled RC frames. All the experimental specimens were subjected to constant vertical load and horizontal cyclic load. Fig. 5 shows the test results and geometric configurations of all the specimens. As shown in Fig. 5(a, b), Huang et al. (Huang et al., 2016) reported cyclic loading tests on a bare RC frame and a RC frame infilled with hollow concrete bricks. Both specimens are one-bay one-story in configuration and designed with 1/2-scale. They had the same height and width of 1375 mm and 2250 mm, respectively. Test results by Huang et al. are indicated as 'Exp1.data' and 'Exp2.data', respectively. As shown in Fig. 5c, Stylianidis (Stylianidis, 2012) conducted quasi-static cyclic loading tests on a 1/3-scale one-bay one-story masonry-infilled RC frame. The specimen had 960 mm in height and 1590 mm in width, respectively. The test result by Stylianidis is indicated as 'Exp3.data'. As shown in Fig. 5d, Lin et al. (Lin et al., 2018) performed cyclic loading tests on a full-scale one-bay one-story masonry-infilled RC frame. The full scale RC frame had 2470 mm in height and 3700mm in width. The test result by Lin et al. is indicated as 'Exp4.data'. The force-displacement curves predicted by the numerical models are also presented in Fig. 5. The test results were plotted with grey solid lines, while the predicted results were plotted with red dash lines. A reasonable agreement was achieved indicating that the macro numerical model can capture the hysteretic behavior of RC frames with and without masonry infills.

Moreover, the energy dissipation in every loading cycle and the accumulated energy dissipation of the specimens are shown in Fig. 6. It is shown that the numerical models may overestimate or underestimate the energy dissipation of test specimens in a single loading cycle, however, the numerical models always can well predict the accumulated energy dissipation of test specimens. Since the accumulated energy dissipation capacity of structural elements under earthquakes is a primary characteristic, it is believed that the proposed numerical model can capture the behavior of bare and masonry-infilled RC frames under earthquakes.

3. Prototype RC frames with masonry infills

As shown in Fig. 7, a 6-story RC frame with four bays (4@ 5.0 m) and two bays (2@ 6.0 m) in each planar direction was selected as the prototype building in the current study. This prototype building was designed in accordance with the seismic design code (GB50011-2010) (GB 50011-2010, 2010) and was assumed to be constructed in the region with a seismic intensity of 8 and a characteristic period of 0.55s. A planar frame in the middle region, shadowed in Fig. 7, was numerically simulated in the current study.

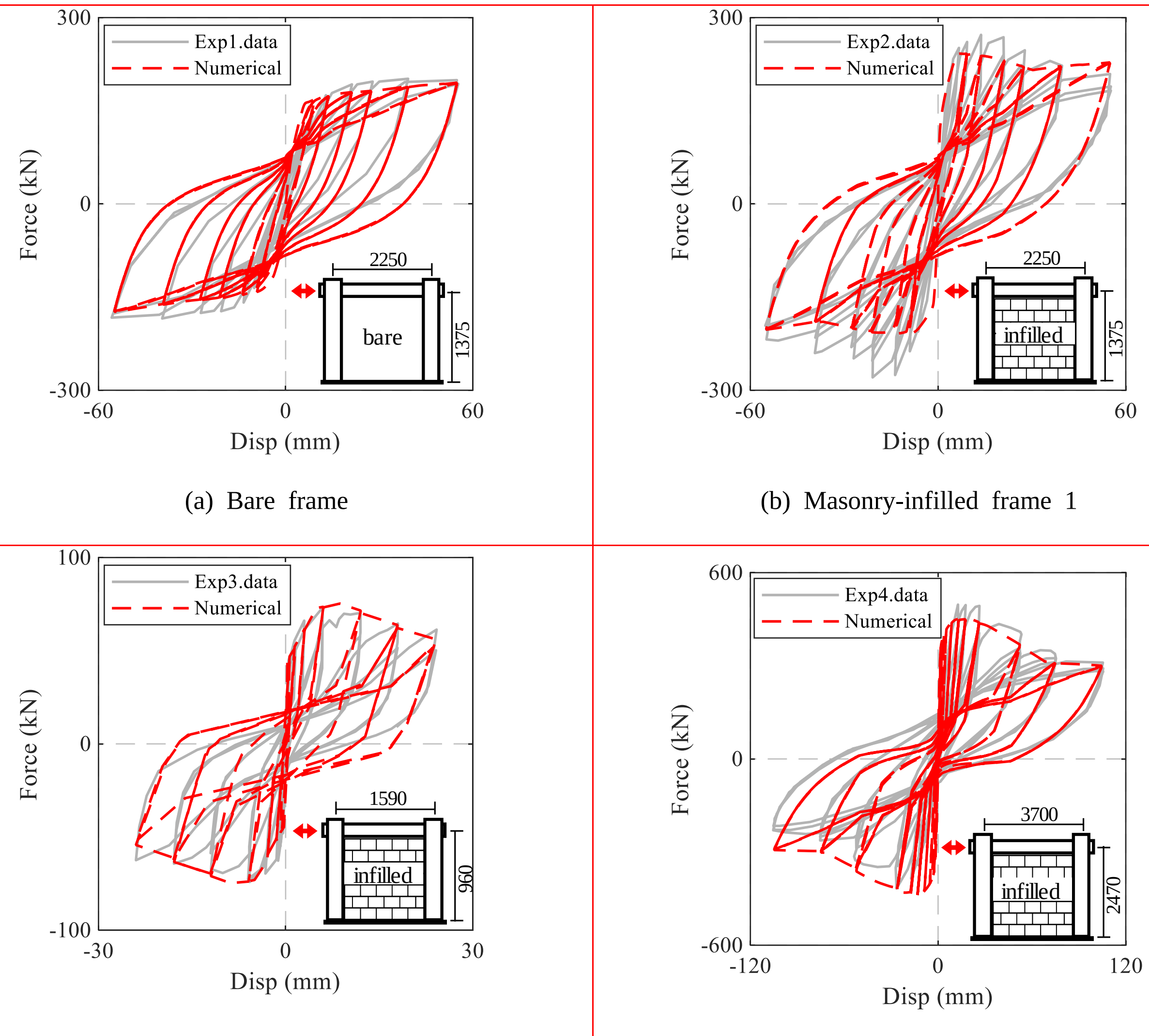

(a) Bare frame

(b) Masonry-infilled frame 1

(c) Masonry-infilled frame 2

(d) Masonry-infilled frame 3

Fig. 5 Force-displacement curves of numerical models and test specimens

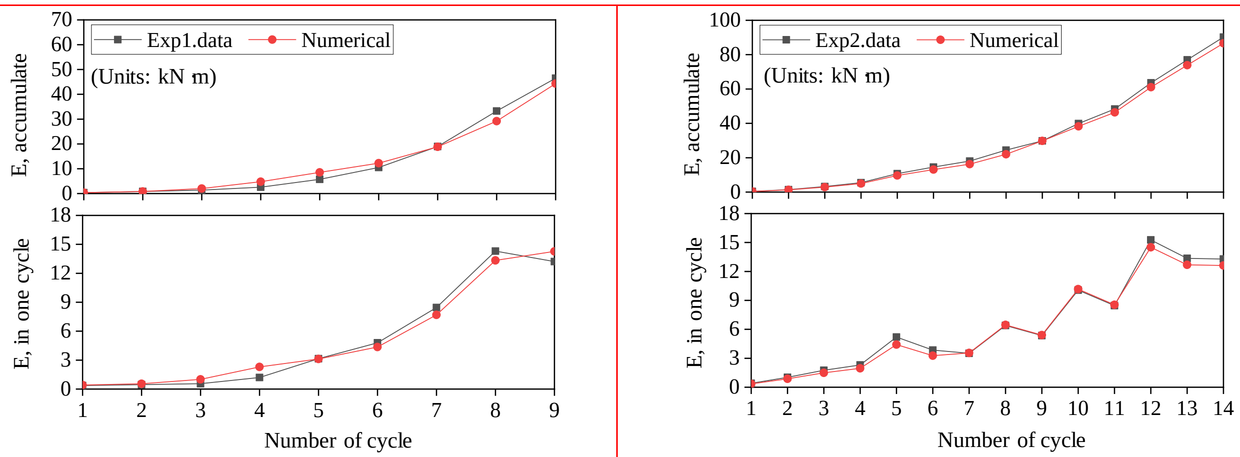

(a) Bare frame

(b) Masonry-infilled frame 1

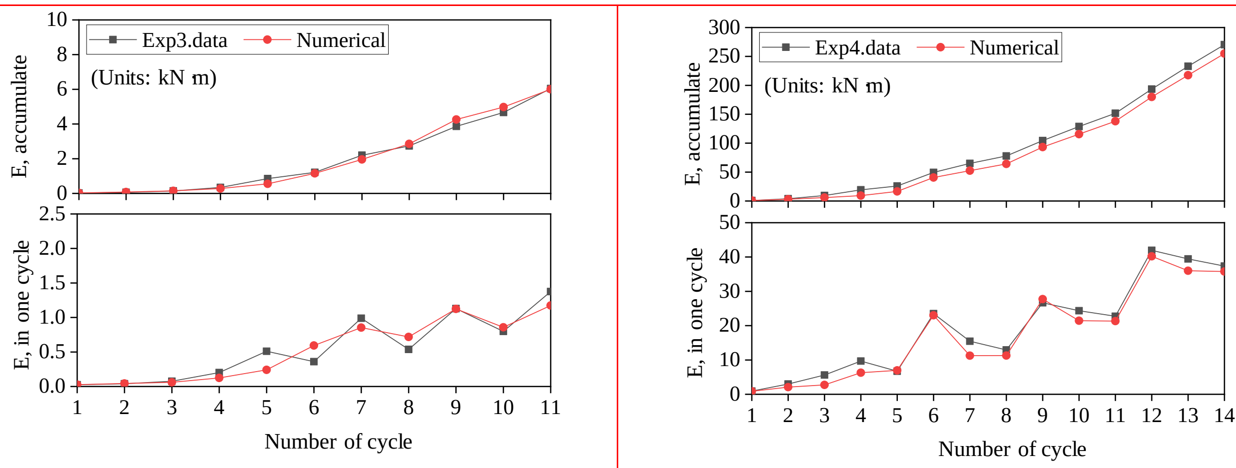

(c) Masonry-infilled frame 2

(d) Masonry-infilled frame 3

Fig. 6 Energy dissipation of numerical models and test specimens

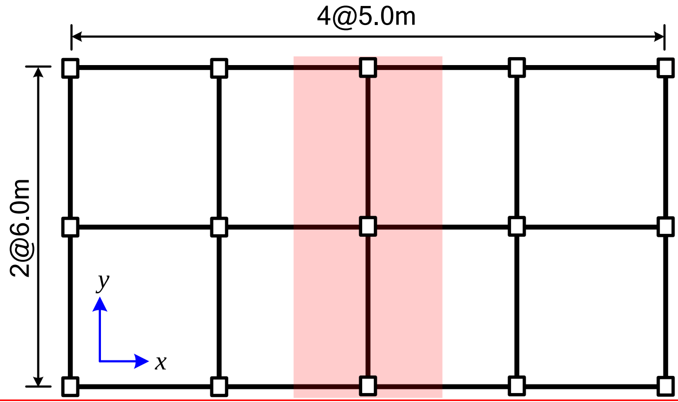

Fig. 7 Plan view of prototype RC frame

As shown in Fig. 8, six distribution scenarios of masonry infill (M1-M6) in the elevation of the prototype frame were considered, including full infilled (M1), open first story (M2), open second story (M3), open the same bay in ground two stories (M4), open different bays in ground two stories (M5) and a bare frame (M6). The first story has a height of 4.2 m and the other stories are 3.5 m in height. The columns of the 6-story frame have the same size of 550 mm × 550 mm. Frame beams have the same size of 300 mm × 550 mm. The design compressive strength of concrete and yield strength of rebar are 30 MPa and 400 MPa, respectively. The dead load and live load on each floor of the frame are 5.0 kN/m2 and 2.0 kN/m2, respectively. The prism compressive strength σ_m0 and bed-joint sliding shear strength τ_m0 of the masonry infills are set as 8.07 and 0.24 MPa, respectively, with reference to ASCE 41-13 (ASCE/SEI, 2013). Table 1 lists the detailed design information of the six RC frames, including the reinforcement ratio of columns and beams, strong-column weak-beam (SCWB) ratio and fundamental periods. As shown in the table, all the frames have the same SCWB ratio of 1.25, while the fundamental periods vary from frame to frame, since the presence of masonry infills alters the elastic stiffness of the RC frames.

4. Seismic collapse risk assessment

4.1 Overview of the methodology

Seismic fragility analysis is a probabilistic based method for identifying collapse risk of a structural system under seismic effects (Cornell et al., 2002). The term ‘fragility’ is quantified as the conditional probability of the structural engineering demand parameter (EDP) exceeding a specific limit state under a given seismic intensity measure (IM). In practice, the maximum inter-story drift ratio (IDRmax) and the spectral acceleration of ground motions at the structural fundamental period Sa(T_1) are widely adopted as the EDP and IM, respectively. The seismic fragility of a structure can be described by the fragility curves. Several approaches, including empirical, judgmental and analytical approaches, can be used to obtain the fragility curves. Assuming the EDPs and IMs are logarithmic correlated (Cornell et al., 2002), they can be expressed as,

$$EDP = a(IM)^b \ or \ \ln(EDP) = \ln(a) + b\ln(IM) \quad (7)$$

where a and b are the regression coefficients. Using the least-square method to fit the data obtained from nonlinear time history analyses (NTHAs), the dispersion of the EDPs at a given IM can be obtained,

$$\beta_{EDP|IM} = \sqrt{\frac{\sum_{i=1}^{N}\left[\ln(EDP) - \ln\left(aIM^b\right)\right]^2}{N-2}} \quad (8)$$

Then, assuming a lognormal distribution for the damage limit states, the seismic fragility defined as the conditional

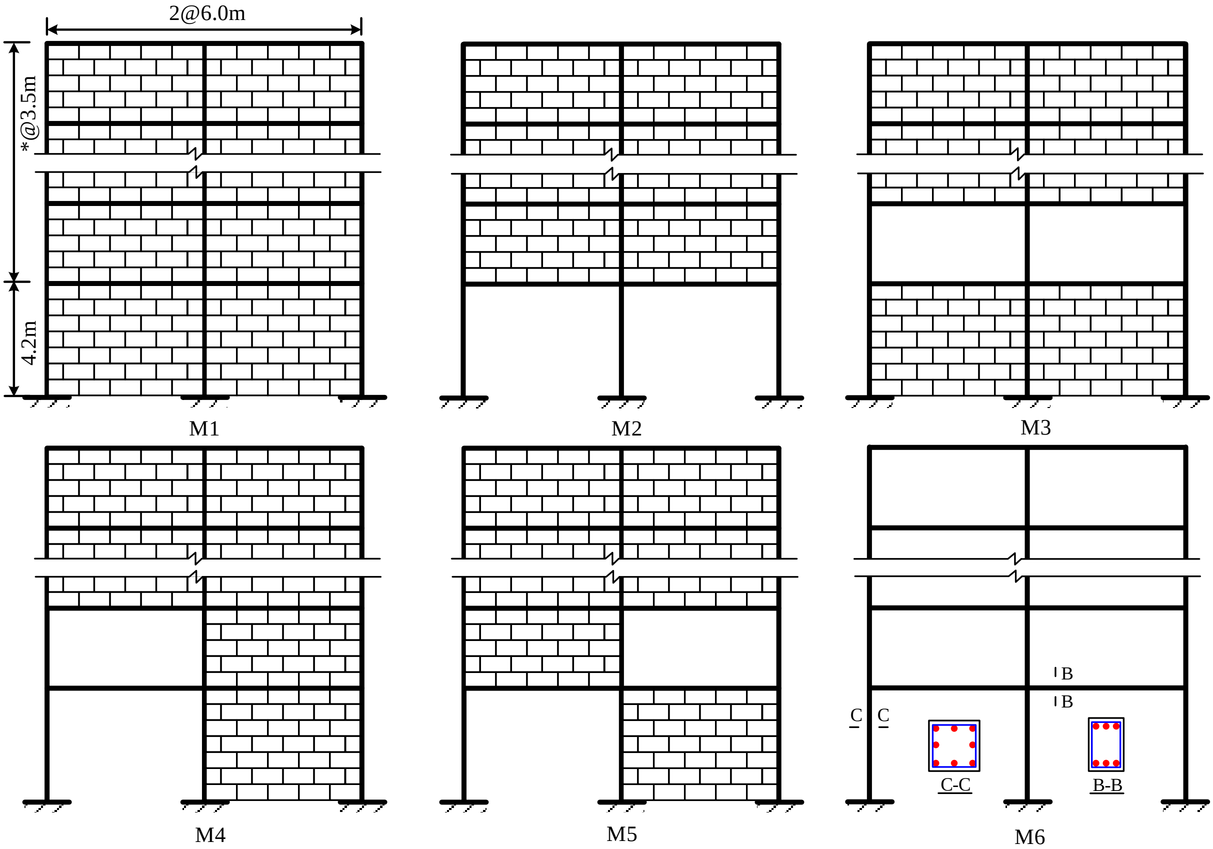

Fig. 8 Distribution scenarios of masonry infills

Table 1 Design information of six masonry-infilled RC frames

No	$B_{col} \times H_{col}$ mm×mm	ρ_{col} * %	$B_{beam} \times H_{beam}$ mm×mm	ρ_{beam}* %	SCWB* ratio	Infill scenario	T_1* (sec.)
1	550×550	0.33	300×550	1.52/0.91	1.25	M1	0.5666
2	550×550	0.33	300×550	1.52/0.91	1.25	M2	0.8829
3	550×550	0.33	300×550	1.52/0.91	1.25	M3	0.8569
4	550×550	0.33	300×550	1.52/0.91	1.25	M4	0.6906
5	550×550	0.33	300×550	1.52/0.91	1.25	M5	0.6811
6	550×550	0.33	300×550	1.52/0.91	1.25	M6	1.0835

*Note: ρ_{col} and ρ_{beam} are the reinforcement ratio of columns and beams, respectively; SCWB ratio is the strong column-weak beam ratio; T_1 is the fundamental period of the frame.

probability of exceeding a certain level of damage state for a given IM, can be expressed as,

$$P[D \geq C \mid IM] = \Phi\left[\frac{\ln(EDP_D / EDP_C)}{\sqrt{\beta_{EDP|IM}^2 + \beta_C^2 + \beta_M^2}}\right] \quad (9)$$

where $\Phi[*]$ is the standard normal cumulative distribution function; β_C is the dispersion of damage states; β_M is the modelling uncertainty (Celik and Ellingwood, 2010). Note that all the modelling parameters for material uncertainties, i.e. masonry infills and boundary frames, are listed in Table 2. Substituting Eq.(7) into Eq.(9), then, Eq.(9) can be rearranged as,

$$P\left[D \geq C \mid IM\right] = \Phi\left[\frac{\ln(IM) - \ln(IM_0)}{\beta_{IM}}\right] \tag{10}$$

wherein,

$$IM_0 = \exp\left[\frac{\ln(EDP_C) - \ln(a)}{b}\right] \tag{11}$$

$$\beta_{IM} = \frac{\sqrt{\beta^2_{EDP|IM} + \beta^2_C + \beta^2_M}}{b} \tag{12}$$

where IM_0 and β_{IM} are the median and dispersion of the fragility curves at a given limit state, respectively. Based on this methodology, probabilistic seismic demand models (PSDMs) of the prototype RC frames can be established using the calculated data from extensive nonlinear time history analyses (NTHAs).

Table 2 Modelling parameters for material uncertainties

Component	Random variables	Mean (MPa)	Coefficient of variation	Distribution
Infill (ASCE)	Prism compressive strength σ_{m0}	8.07 (ASCE/SEI, 2013)	0.200	Lognormal
	Bed-joint sliding shear strength τ_{m0}	0.24 (ASCE/SEI, 2013)	0.267	Lognormal
Boundary frame	Concrete compressive strength f_c	30 (GB50010-2010)	0.150	Normal
	Rebar yield strength f_y	400 (GB50010-2010)	0.110	Lognormal

4.2 Uncertainty model

Based on the numerical models of the prototype masonry-infilled RC frames (Fig. 4), uncertainty models were developed considering material uncertainties in the masonry infills and the boundary frames. For instance, uncertainties in the prism compressive strength (f_m), bed-joint sliding shear strength (τ_0), and diagonal shear strength (τ_d) for masonry infills, steel yield strength (f_y) and concrete compressive strength (f_c) for the boundary frames are incorporated in the frame models with the Latin Hypercube Sampling (LHS) method (Celik and Ellingwood, 2010). Key parameters for the material uncertainties, including mean value, coefficient of variation and probabilistic distributions, are listed in Table 2. According to ASCE 41-13 (ASCE/SEI, 2013), the elastic modulus (E_m) and the shear modulus (G_m) of the infill are functions of the prism compressive strength f_m, (i.e. E_m/f_m =550, G_m/E_m =0.4). Thus, this study assumes that the uncertainty in these two moduli depend on the prism compressive strength.

Nonlinear time history analysis of the prototype RC frames was performed using a set of 22 far-field ground motions recommended in FEMA P695 (Federal Emergency Management, 2009) to explicitly account for the uncertainty in ground motions, as listed in Table 3. Each ground motion record has two horizontal components, and the one that can better match the design spectrum was adopted. Thus the uncertainties inherent in the earthquake loading were taken into account. The response spectrum of each record and average spectrum with 5% damping are shown in Fig. 9. In addition, the design spectrum of the prototype building under maximum considered earthquake (i.e. rare earthquake) is illustrated in the figure. As shown, the Average spectrum of the selected ground motions (GM01-GM22) can generally match the design spectrum very well. Moreover, this ground motion suite has been widely adopted to assess the seismic performance of structures (Federal Emergency Management, 2009; Li et al. 2018; Li et al. 2019), and therefore the results and conclusions reached in this study is expected to be easy to understand and accept in research communities and industries.

4.3 Fragility curves based on IDA results

This study employs the analytical based method to obtain the fragility curves of the RC frames with various distribution patterns of masonry infills. Incremental dynamic analysis (IDA) has been widely adopted in seismic performance evaluation of structural system since first proposed by Vamvatsikos and Cornell (Vamvatsikos and Cornell, 2002). In the current study, 22 IDA curves of each RC frame model under the scaled ground motions were obtained through hundreds of nonlinear time history analyses results.

Table 3 Selected seismic ground motions

No.	NGA #	Earthquake Record	Moment Magnitude	PGA(g)
GM01	953	Northridge,1994	6.7	0.42

GM02	960	Northridge,1994	6.7	0.48
GM03	1602	Duzce,Turkey,1999	7.1	0.73
GM04	1787	Hector Mine,1999	7.1	0.27
GM05	169	Imperial Valley,1979	6.5	0.24
GM06	174	Imperial Valley,1979	6.5	0.38
GM07	1111	Kobe, Japan, 1995	6.9	0.50
GM08	1116	Kobe, Japan, 1995	6.9	0.24
GM09	1158	Kocaeli,Turkey,1999	7.5	0.31
GM10	1148	Kocaeli,Turkey,1999	7.5	0.15
GM11	900	Landers, 1992	7.3	0.15
GM12	848	Landers, 1992	7.3	0.42
GM13	752	Loma Prieta, 1989	6.9	0.53
GM14	767	Loma Prieta, 1989	6.9	0.56
GM15	1633	MANJIL, 1990	7.4	0.50
GM16	721	Superstition Hills,1987	6.5	0.26
GM17	725	Superstition Hills,1987	6.5	0.45
GM18	829	Cape Mendocino, 1992	7.0	0.55
GM19	1244	Chi-Chi, Taiwan, 1999	7.6	0.44
GM20	1485	Chi-Chi, Taiwan, 1999	7.6	0.47
GM21	68	San Fernando, 1971	6.6	0.21
GM22	125	Friuli, Italy, 1976	6.5	0.31

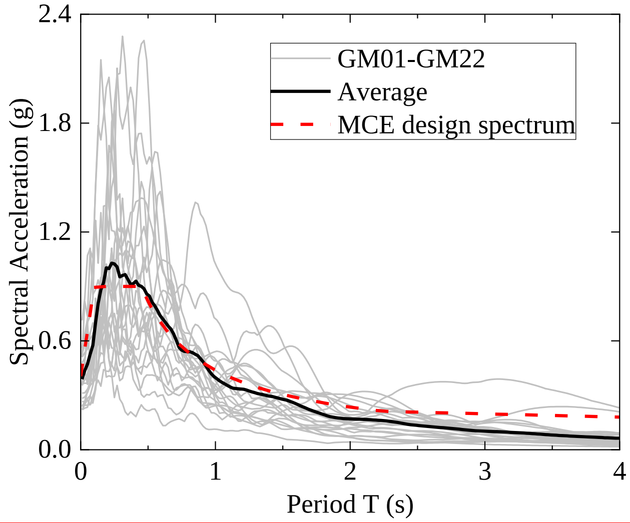

Fig. 9 Spectrums of seismic ground motions

Fig. 10 shows IDA results of the six masonry-infilled RC frames. There was no significant difference in the lower bound of intensity measure, Sa(T_1), for all scenarios, while the upper bound of Sa(T_1) ranged from 1.8 g to 3.0 g. The limit states defined in FEMA 356 (ASCE, 2000) together with the IDA results were adopted to develop the collapse fragility curves in this study. The FEMA 356 standard is one of the most important standard for structural seismic performance evaluation and rehabilitation. In this standard, the building performance is expressed in terms of target building performance levels. Three target building performance levels are specified, including “immediate occupancy” (IO) with a drift ratio limit of 1.0%, “life safety” (LS) with a drift ratio limit of 2.0% and “collapse prevention” (CP) with a drift ratio limit of 4.0%. The IO performance level corresponds to a damage state that minor hairline cracking, or limited yielding possible at a few locations and no crushing (strains below 0.003). The LS performance level corresponds to a damage state that extensive damage to beams, or spalling of cover and shear cracking (<1/8" width) for ductile columns. Minor spalling in nonductile columns and joint cracks <1/8" wide. The CP performance level corresponds to a damage state that Extensive cracking and hinge formation in ductile elements. Limited cracking and/or splice failure in some nonductile columns. The fragility curves of masonry-infilled RC frames (M1-M6) at the three damage limit states are shown in Fig. 11. As shown, the existence of masonry infills generally reduces the probability of collapse of the RC frames across all the damage states from IO to CP, except the open first story scenario (M2). The masonry-infilled RC frames with open first story is most vulnerable to the seismic effect, while the RC frame with full masonry infills (M1) is least sensitive to the seismic effect among all the scenarios. In other words, the bare frame (M6) is effectively strengthened by the fully distributed masonry infills, therefore the collapse risk is significantly reduced. For the RC frame with open first story (M2), lateral stiffness and strength of the upper stories are significantly higher than the first story, thus the first story becomes the softest/weakest story. Under earthquakes, inter-story drifts tend to concentrate in the softest/weakest story, thereby it may result in a weak story failure. It is noteworthy that the continuous and staged opening in one bay of the first two stories (i.e., M4 and M5) have no significant difference in collapse risk. This phenomenon can be owned to the fact that for the low rise RC frames, shear deformation mainly occurs under horizontal action, such as earthquakes, while the flexural deformation is negligible.

The middle value of the horizontal axis $Sa(T_1)$, 0.5g, is also indicated in Fig. 11. Under this seismic intensity, the bare frame (M6) has a probability of damage of 92%, 39% and 14% for IO, LS and CP limit states, respectively. While the open ground story frame (M2) has a probability of damage of 95%, 44% and 17% for IO, LS and CP limit states; the full infilled frame (M1) has a probability of damage of 37%, 2% and 0.7% for IO, LS and CP limit states, respectively.

As shown in Table 4, the different frame models are compared by the median value of the fragility curves $Sa(T_1)_m$, which is the $Sa(T_1)$ value associated with a 50% probability of exceeding a given limit state. For simplicity, the relative fragility of all the models is examined with respect to the bare frame model. Specifically, $Sa(T_1)_m$ of IO is 0.96 to 1.92 times those of the bare frame; $Sa(T_1)_m$ of LS is 0.95 to 1.76 times those of the bare frame; and $Sa(T_1)_m$ of CP is 0.97 to 1.55 times those of the bare frame.

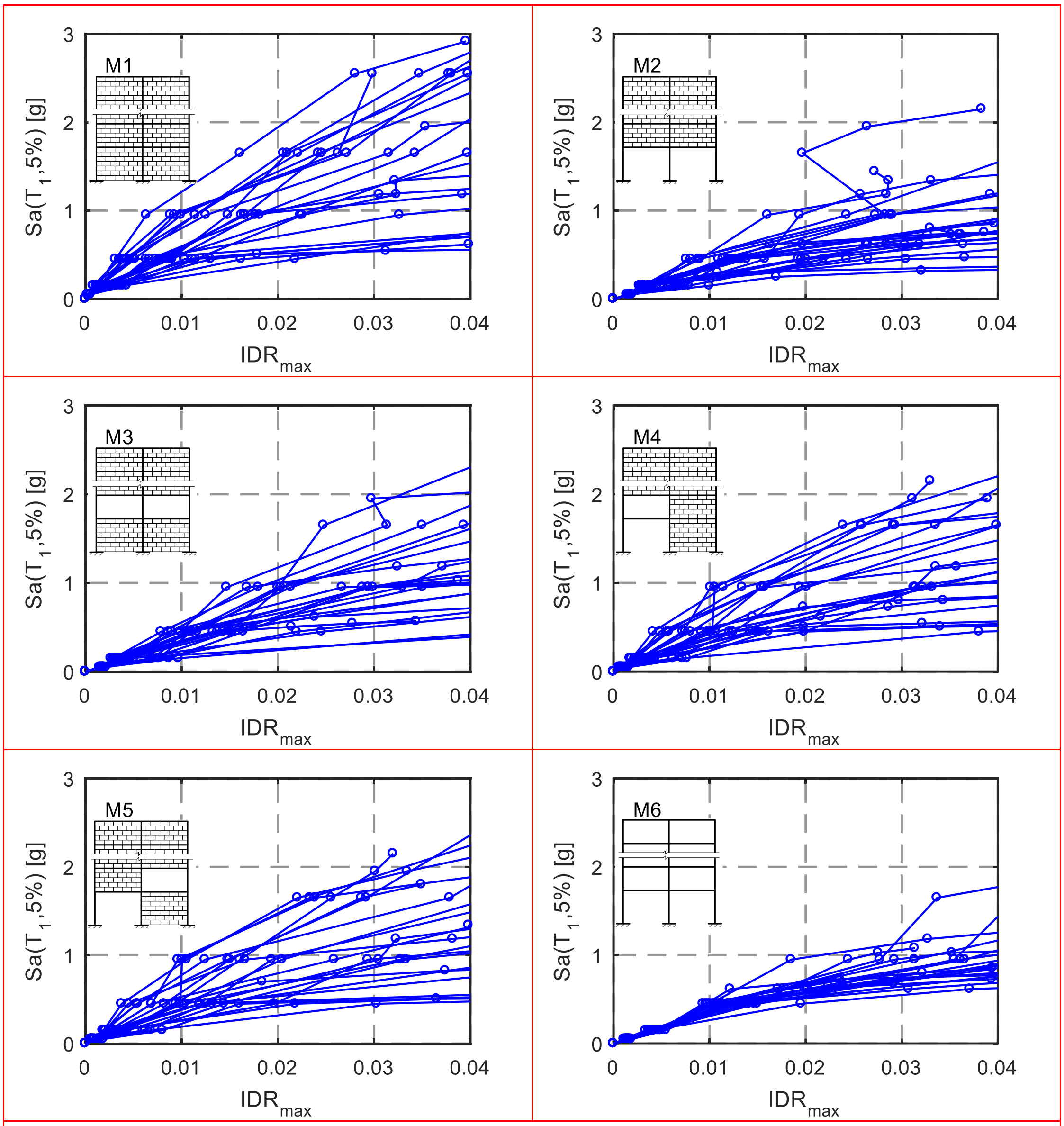

Fig. 10 IDA results of prototype frames

5. Seismic collapse risk assessment

In current seismic design codes (ACI318-14, 2014; GB 50011-2010, 2010), the strong-column weak-beam ratio (SCWB) is the design parameter that controls the structural global behavior under earthquakes, which is defined as,

$$\eta_{cb} = \sum M_{nc} / \sum M_{nb} \tag{13}$$

where $\sum M_{nc}$ is the sum of nominal flexural strength of the columns framed into the joint which are evaluated at the faces of the joint; $\sum M_{nb}$ is the sum of nominal flexural strengths of the beams framed into the joint which are evaluated at the faces of the joint. It is specified in GB50011-2010 (GB 50011-2010, 2010), as well as in ACI318-14 (ACI318-14, 2014), that the SCWB ratio should be no less than 1.20 to avoid weak story failure of RC frames.

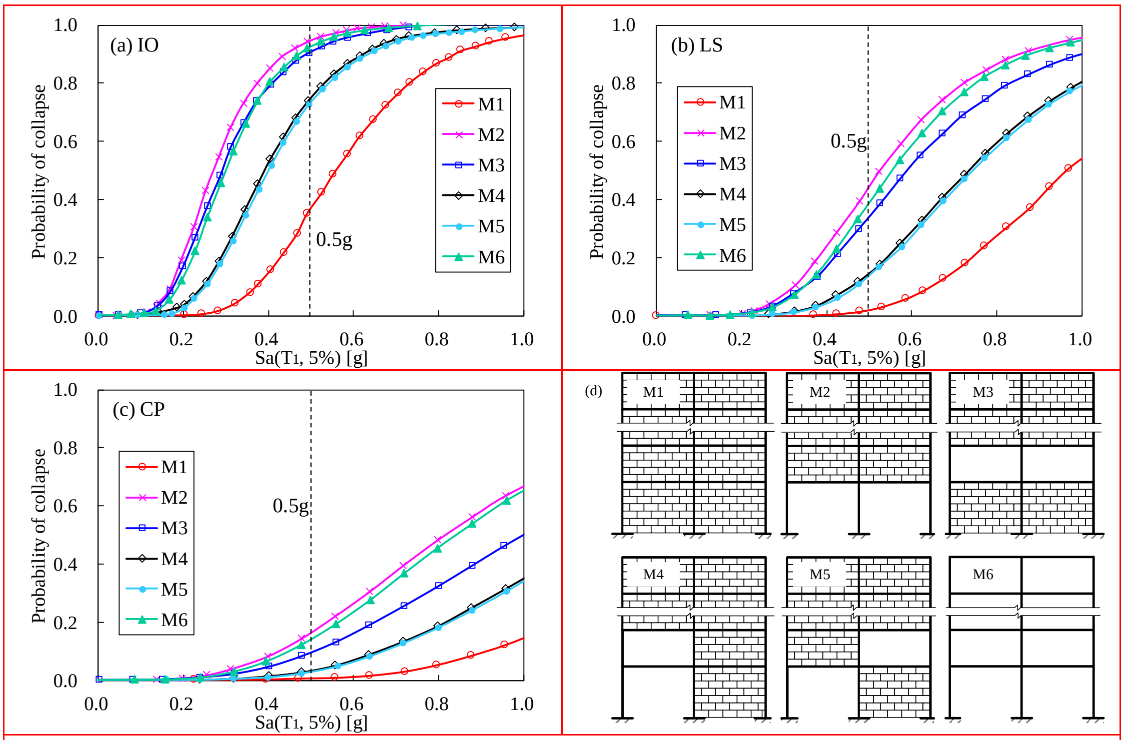

Fig. 11 Comparison of fragility curves: (a) IO state, (b) LS state, (c) CP state, (d) M1-M6

Table 4 Median values of fragility curves Sa(T_1) for all frame models

Frame	$Sa(T_1)_m$ [g]			$Sa(T_1)_{m,infill}$ / $Sa(T_1)_{m,bare}$		
	IO	LS	CP	IO	LS	CP
M1	0.560	0.977	1.543	1.92	1.76	1.55
M2	0.279	0.528	0.966	0.96	0.95	0.97
M3	0.300	0.590	1.053	1.03	1.06	1.06
M4	0.392	0.729	1.222	1.35	1.31	1.23
M5	0.401	0.743	1.246	1.38	1.33	1.25
M6	0.291	0.557	0.993	1.00	1.00	1.00

As reported in the literature (Haselton et al., 2011), increasing the required SCWB ratio of RC frames delays the formation of plastic hinges in columns, thus increasing both the number of stories involved in the collapse mechanism and inelastic deformation capacity of the entire frame under earthquakes. To quantify the effect of SCWB ratio, the prototype RC frames (M1-M6) were investigated with the SCWB ratio ranging from 0.8 to 2.0.

Fig. 12 shows the envelope of maximum inter-story drift distributions of the frames with SCWB ratios of 0.8 and 2.0, respectively, subject to ground motions listed in Table 3. The mean spectral value of input ground motions at structure fundamental period was amplified to match the rare earthquake intensity in GB50011-2010 (GB 50011-2010, 2010). As shown in the figure, the inter-story drifts tend to concentrate in the ground story for most frames with an SCWB ratio of 0.8, except for the open second story scenario (M3). For the frames with an SCWB ratio of 2.0, both the maximum value and concentration of the inter-story drifts were significantly reduced for all the scenarios.

This phenomenon can be attributed to two reasons. Firstly, the increment of SWCB ratio was obtained by increasing the reinforcement ratio of frame columns and hence the structural system capacity was improved rapidly, therefore the maximum inter-story drifts were reduced. Secondly, since the flexural strengths of the column ends are much higher than those of the beam ends at high SCWB ratio, the frame with opening story, such as M2 and M3, tended to form plastic hinges at beam ends rather than at the columns. Fig. 13 shows the distribution of plastic hinges of M2 and M3 models subject to ground motion record GM02 (i.e. Northridge, 1994). Note that the distribution of plastic hinges was obtained from the nonlinear time history analysis results when the recorded bending maximum moment reached the section flexural strength. Referring to Fig. 4, nonlinear fiber elements were adopted to simulate the hysteretic behavior of structural elements and the flexural strength is defined as the bending moment at the ends of frame beams and columns when the steel reinforcement fibers yield.

To quantify the inter-story drifts response, the mean value of the envelope inter-story drift response was adopted as,

$$\overline{IDR_{\max,i}} = \frac{1}{22}\sum_{j=1}^{22} IDR_{\max,ij} \ \left(i=1,\ldots,n\right) \tag{14}$$

where $IDR_{\max,ij}$ is the maximum drift ratio of ith story of RC frames subjected to jth ground; n is the number of stories.

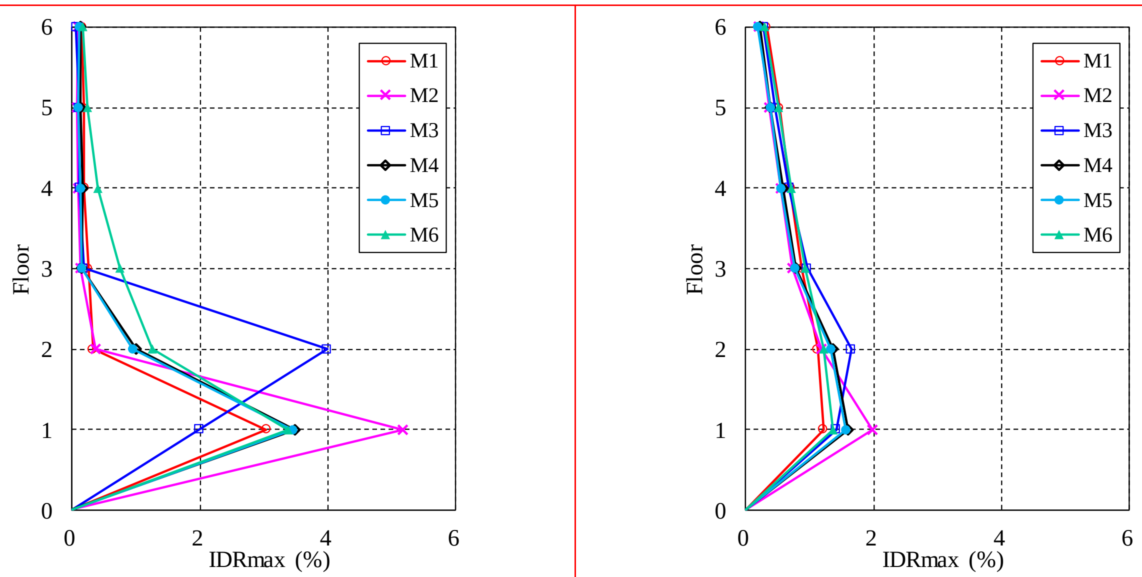

(a) SCWB ratio of 0.8

(b) SCWB ratio of 2.0

Fig. 12 Comparison of maximum inter-story drift distribution

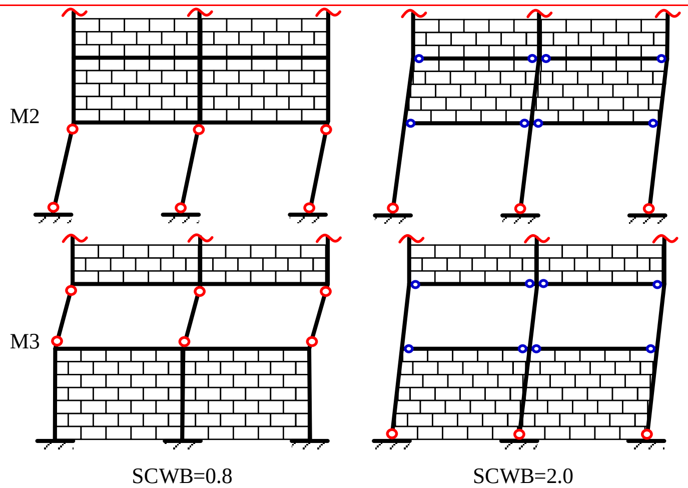

Fig. 13 Comparison of plastic hinge distribution in RC frames

The mean value of maximum inter-story drift ratio of all the stories under a certain seismic intensity is defined as,

$$\overline{IDR}_{\max} = \frac{1}{n}\sum_{i=1}^{n}\overline{IDR}_{\max,i} \tag{15}$$

A drift concentration index is defined to quantify the inhomogeneity of maximum inter-story drift responses as,

$$\beta = \frac{\max(\overline{IDR}_{\max,i})}{\overline{\overline{IDR}}_{\max}} \; (i = 1, \ldots, n) \tag{16}$$

Fig. 14 shows the drift concentration index for all six scenarios with SCWB ratios ranging from 0.8 to 2.0. The variation of SCWB ratios was obtained by adjusting the reinforcement ratio of the columns. In general, the drift concentration index β_w reduced rapidly with increasing SCWB ratios. The frame with open ground story (M2) has the highest drift concentration index over the considered SCWB ratio range. As the SCWB ratio increased from 0.8 to 2.0, the β_w reduced from 5.9 to 2.4. The frames with continuous and staged opening at the ground two stories (i.e., M4 and M5) have almost the same drift concentration index, which was reduced from 4.8 to 1.9 with the increment of SCWB ratios. For the SCWB ratio range of 0.8 to 1.25, the drift concentration index of all scenarios were well above 3.0, despite the bare frame M1, which reduced to 2.97 at a SCWB ratio of 1.25. In order to achieve the same drift concentration index as the bare frame, the SCWB ratios of other scenarios should be no less than 1.5. For the open ground story scenario M2, this value may be as high as 1.8.

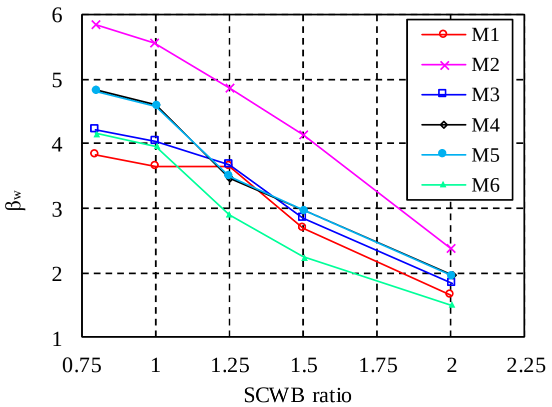

Fig. 14 Effect of SCWB ratios on drift concentration index

6. Conclusions

The seismic collapse risk of reinforced concrete (RC) frames with irregular distributed masonry infills were assessed through large number of nonlinear time history analyses (NTHAs). Based on the results of NTHAs, seismic fragility curves were obtained for each frame model. The uncertainties in material properties and ground motions were considered. The effect of strong-column weak-beam (SCWB) ratio on the inter-story drift concentration and seismic failure mechanism was investigated through parametric studies. The following conclusions can be drawn:

- The existing of masonry infills generally reduces the seismic collapse risk of the RC frames across all the damage states from immediate occupancy to collapse prevention, except the open first story scenario (M1), which tends to form a weak story failure.
- The masonry-infilled RC frames with open first story (M2) is most vulnerable to the seismic effect, while the RC frame with fully masonry infills (M1) is least sensitive to the seismic effect among all the scenarios. In particular, the continuous (M4) and staged opening (M5) in one bay of the ground two stories have no significant difference in collapse risk.
- Improving the strong - column weak - beam (SCWB) ratio of the RC frames with irregular distributed masonry infills can reduce inter-story drift concentration under earthquakes. To achieve the same drift concentration index of bare RC frame with SCWB ratio about 1.2, the SCWB ratio should be no less than 1.5. For the open first/ground story scenario M2, this value may be as high as 1.8.

Acknowledgments

The work presented in this paper was supported by the Fundamental Research Funds for the Central Universities with project number 2018CDJSK03XK03 and the National Science Foundation for Young Scientists of China with project number 51808068.

References

ASCE/SEI. (2013). Seismic evaluation and retrofit of existing buildings (ASCE/SEI 41-13). American Society of Engineers. https://doi.org/10.1061/9780784412855

ASCE, FEMA 356. (2000). Prestandard and commentary for the seismic rehabilitation of buildings. Report FEMA-356, Washington, DC. https://www.fema.gov/media-library-data/20130726-1444-20490-5925/fema_356.pdf

ASCE7-10. (2016). Minimum Design Loads for Buildings and Other Structures. . In Minimum Design Loads for Buildings and Other Structures. American Society of Civil Engineers. https://doi.org/10.1061/9780784414248

Asteris, P G, Repapis, C. C., Foskolos, F., Fotos, A., & Tsaris, A. T. (2017). Fundamental period of RC frame structures with veritcal irregularity. Structural Engineering and Mechanics, 61(5), 663–674. https://doi.org/10.12989/sem.2017.61.5.663

Asteris, Panagiotis G., Repapis, C. C., Cavaleri, L., Sarhosis, V., & Athanasopoulou, A. (2015). On the fundamental period of infilled RC frame buildings. Structural Engineering and

Mechanics, 54(6), 1175–1200. http://dx.doi.org/10.12989/sem.2015.54.6.1175
Bikce, M. (2011). How to reduce short column effects in buildings with reinforced concrete infill walls on basement floors. Structural Engineering and Mechanics, 38(2), 249–259. http://dx.doi.org/10.12989/sem.2011.38.2.249
Burton, H., & Deierlein, G. (2014). Simulation of Seismic Collapse in Nonductile Reinforced Concrete Frame Buildings with Masonry Infills. JOURNAL OF STRUCTURAL ENGINEERING, 140(8), A4014016. http://dx.doi.org/10.1061/(ASCE)ST.1943-541X.0000921
Celik, O. C., & Ellingwood, B. R. (2010). Seismic fragilities for non-ductile reinforced concrete frames–Role of aleatoric and epistemic uncertainties. Structural Safety, 32(1), 1–12. http://dx.doi.org/10.1016/j.strusafe.2009.04.003
Chao, L., Zixiong, G., Qunxian, H., Qunxian, H., Zhenling, C., Yang, L. (2018). Experimental study on seismic behavior of full-scale infilled RC frames. Journal of Building Structures (In Chinese), 39(09), 30–37. http://dx.doi.org/10.14006/j.jzjgxb.2018.09.004
ACI 318-14. (2014). Building code requirements for structural concrete and commentary. American Concrete Institute. https://www.concrete.org/store/productdetail.aspx?ItemID=318U14&Language=English
Cornell, C. A., Jalayer, F., Hamburger, R. O., Foutch, D. A. (2002). Probabilistic basis for 2000 SAC federal emergency management agency steel moment frame guidelines. JOURNAL OF STRUCTURAL ENGINEERING, 128(4), 526–533. http://dx.doi.org/10.1061/(ASCE)0733-9445(2002)128:4(526)
De Domenico, D., Falsone, G., & Laudani, R. (2018). In-plane response of masonry infilled RC framed structures: A probabilistic macromodeling approach. Structural Engineering and Mechanics, 68(4), 423–442. http://dx.doi.org/10.12989/sem.2018.68.4.423
Eurocode8. (2005). Eurocode 8: Design of structures for earthquake resistance—Part 1, 1991–1998. https://eurocodes.jrc.ec.europa.eu/showpage.php?id=138
FEMA P695. (2009). Quantification of Building Seismic Performance Factors. Federal Emergency Management Agency, Washington, DC. https://www.fema.gov/media-library-data/20130726-1716-25045-9655/fema_p695.pdf
GB50010-2010 (2011). Code for design of concrete structures. https://www.codeofchina.com/standard/GB50010-2010.html
GB 50011-2010, (2010). Code for Seismic Design of Buildings. https://www.codeofchina.com/standard/GB50011-2010(2016).html
Haselton, C. B., Liel, A. B., Deierlein, G. G., Dean, B. S., & Chou, J. H. (2011). Seismic Collapse Safety of Reinforced Concrete Buildings. I: Assessment of Ductile Moment Frames. JOURNAL OF STRUCTURAL ENGINEERING, 137(4), 481–491. http://dx.doi.org/10.1061/(ASCE)ST.1943-541X.0000318
Huang, Q., Guo, Z., Kuang, J. S. (2016). Designing infilled reinforced concrete frames with the ‘strong frame-weak infill’ principle. Engineering Structures, 123, 341–353. http://dx.doi.org/10.1016/j.engstruct.2016.05.024
IBC2000 (2000). International Building Code 2000. Dearborn Trade Publishing. https://archive.org/details/gov.law.icc.ibc.2000/mode/2up
Khoshnoud, H. R., & Marsono, K. (2016). Experimental study of masonry infill reinforced concrete frames with and without corner openings. Structural Engineering and Mechanics, 57(4), 641–656. http://dx.doi.org/10.12989/sem.2016.57.4.641
Li, Y.-W., Li, G.-Q., Jiang, J., & Sun, F.-F. (2018). Mitigating seismic response of RC moment resisting frames using steel energy-dissipative columns. Engineering Structures, 174, 586–600. http://dx.doi.org/10.1016/j.engstruct.2018.07.097
Li, Y.-W., Li, G.-Q., Jiang, J., & Wang, Y.-B. (2019). Seismic performance improvement of tension-only-braced frames with Energy-Dissipative Rocking Columns. Engineering Structures, 196, 109286. https://doi.org/10.1016/j.engstruct.2019.109286
Liberatore, L., & Decanini, L. D. (2011). Effect of infills on the seismic response of high-rise RC buildings designed as bare according to Eurocode 8. Ingegneria Sismica, 3, 7–23. http://ingegneriasismica.org/en/effect-of-infills-on-the-seismic-response-of-high-rise-rc-buildings-designed-as-bare-according-to-eurocode-8/
Mazzoni, S., McKenna, F., Scott, M. H., & Fenves, G. L. (2006). OpenSees command language manual. Pacific Earthquake Engineering Research (PEER) Center. https://opensees.berkeley.edu/OpenSees/manuals/usermanual/OpenSeesCommandLanguageManualJune2006.pdf
Mohammad Noh, N., Liberatore, L., Mollaioli, F., & Tesfamariam, S. (2017). Modelling of masonry infilled RC frames subjected to cyclic loads: State of the art review and modelling with OpenSees. Engineering Structures, 150, 599–621. http://dx.doi.org/10.1016/j.engstruct.2017.07.002
Muthukumar, S., Satyanarayanan, K. S., & Senthil, K. (2017). Studies on two bay and three storey infilled frame with different interface materials: Experimental and finite element studies. Structural Engineering and Mechanics, 64(5), 543–555. https://doi.org/10.12989/sem.2017.64.5.543
Papia, M., Cavaleri, L., & Fossetti, M. (2003). Infilled frames: Developments in the evaluation of the stiffening effect of infills. Structural Engineering and Mechanics, 16(6), 675–693. https://doi.org/10.12989/sem.2003.16.6.675
Paulay, T., & Priestley, M. J. N. (1992). Seismic design of reinforced concrete and masonry buildings. https://doi.org/10.1002/9780470172841
Quayyum, S., Alam, M. S., & Rteil, A. (2013). Seismic behavior of soft storey mid-rise steel frames with randomly distributed masonry infill. Steel and Composite Structures, 14(6), 523–545. https://doi.org/10.12989/scs.2013.14.6.523
Sandhu, B., Sharma, S., & Kwatra, N. (2020). Analysis of behavior of bare and in-filled RC frames subjected to quasi static loading. Structural Engineering and Mechanics, 73(4), 381–395. https://doi.org/10.12989/sem.2020.73.4.381
Scott, M. H., & Fenves, G. L. (2006). Plastic hinge integration methods for force-based beam–column elements. Journal of Structural Engineering, 132(2), 244–252. http://dx.doi.org/10.1061/(ASCE)0733-9445(2006)132:2(244)
Stylianidis, K. C. (2012). Experimental Investigation of Masonry Infilled R/C Frames. Open Construction & Building Technology Journal, 6(1), 194–212. http://dx.doi.org/10.2174/1874836801206010194
Vamvatsikos, D., & Cornell, C. A. (2002). Incremental dynamic analysis. Earthquake Engineering & Structural Dynamics, 31(3), 491–514. http://dx.doi.org/10.1002/eqe.141
Verde, R. V. (1991). Explanation for the numerous upper floor collapses during the 1985 Mexico city earthquake. Earthquake Engineering & Structural Dynamics, 20(3), 223–241. https://doi.org/10.1002/eqe.4290200303
Yuen, Y. P., & Kuang, J. S. (2015). Nonlinear seismic responses and lateral force transfer mechanisms of RC frames with different infill configurations. Engineering Structures, 91, 125–140. https://doi.org/10.1016/j.engstruct.2015.02.031
Zhao, B., Taucer, F., & Rossetto, T. (2009). Field investigation on the performance of building structures during the 12 May 2008 Wenchuan earthquake in China. Engineering Structures, 31(8), 1707–1723. https://doi.org/10.1016/j.engstruct.2009.02.039